

# Structural Heterogeneity and Bioimaging of S100 Amyloid Assemblies

Sofia B. Carvalho<sup>1</sup>, Isabel Cardoso<sup>2,3</sup>, Hugo M. Botelho<sup>1,#</sup>, Kiran Yanamandra<sup>4,+</sup>, Günter Fritz<sup>5</sup>, Cláudio M. Gomes<sup>1,\*</sup>, Ludmilla A. Morozova-Roche<sup>4,\*</sup>

<sup>1</sup>Instituto Tecnologia Química e Biológica, Universidade Nova de Lisboa, Oeiras, Portugal, <sup>2</sup>Molecular Neurobiology Unit, Instituto de Biologia Molecular e Celular, Porto, Portugal, <sup>3</sup>Escola Superior Tecnologia Saúde Porto, Instituto Politécnico do Porto, Vila Nova de Gaia, Portugal, <sup>4</sup>Department of Medical Biochemistry and Biophysics, Umeå University, Sweden, <sup>5</sup>Department of Neuropathology, University of Freiburg, Germany, #current address: BioISI - Biosystems & Integrative Sciences Institute, Faculty of Sciences, University of Lisboa, Portugal, +current address: Department of Neurology, Washington University School of Medicine, St. Louis, USA

\*Corresponding authors (gomes@itqb.unl.pt and ludmilla.morozova-roche@medchem.umu.se)

## Chapter Outline

<b>Introduction</b>	<b>197</b>	Sources of Amyloid – <i>In Vivo</i> and <i>In Vitro</i>	203
<b>Structural Diversity of S100 Monomers and Multimers</b>	<b>198</b>	S100A8/A9 Amyloids	203
S100 Structure and Folding	198	Amyloidogenic Properties of S100A6 Studied by TEM	204
Ca <sup>2+</sup> and Other Metal-Binding Properties	199	S100B Amyloid Formation <i>In Vitro</i>	206
<b>S100 Oligomers, Aggregates and Amyloids</b>	<b>200</b>	<i>Ex Vivo</i> S100A8/A9 Amyloids Imaged by	
S100 Functional Oligomers	200	AFM and TEM	207
Amyloidogenic and Aggregation Potential of S100 Proteins	201	Macroscopic Amyloid Properties of <i>Corpora Amylacea</i>	
Effects of S100 on Aggregation Cross-Seeding	201	Studied by Optical Microscopy	208
Role of Metal Ions in Aggregation Pathways	202	<b>Conclusions</b>	<b>209</b>
<b>Bioimaging of S100 Amyloids by AFM and TEM</b>	<b>202</b>	Abbreviations	209
Techniques to Study Protein Amyloid Formation	202	<b>Acknowledgments</b>	<b>209</b>

## INTRODUCTION

S100 proteins are Ca<sup>2+</sup>- and Zn<sup>2+</sup>-binding proteins that constitute the largest subgroup within the superfamily of Ca<sup>2+</sup>-binding EF-hand proteins. In humans, 21 members have been identified so far [1,2]; these show a tissue- and cell-type-specific expression pattern and characteristic subcellular localizations [3]. S100 proteins became the focus of intensive research owing to their association with numerous human disorders, including acute and chronic inflammatory conditions, autoimmune diseases, cancer, atherosclerosis, cardiomyopathies and neurodegenerative diseases [4-8], apart from their crucial roles in cell physiology. These proteins are able to perform a plethora of intra- and extracellular functions, including cytokine-like and chemokine-like

activities via activation of the receptor for advanced glycation endproducts (RAGE) [9] and toll-like receptor 4 (TLR4)-dependent signalling cascades [10], regulation of the cytoskeleton via tubulin polymerization [11] and other functions. Recently, a new property among S100 proteins was unveiled: we have discovered that the S100A8/A9 proteins form amyloids both in the aging prostate and *in vitro* [12]. Amyloidogenic propensity *in vitro* is also shared by other S100 proteins [13], including S100A6 [14]. Here, we review and discuss the conformational plasticity of S100 proteins, which may underlie their multiple pathways of self-assembly leading to their multiple roles in health and disease.

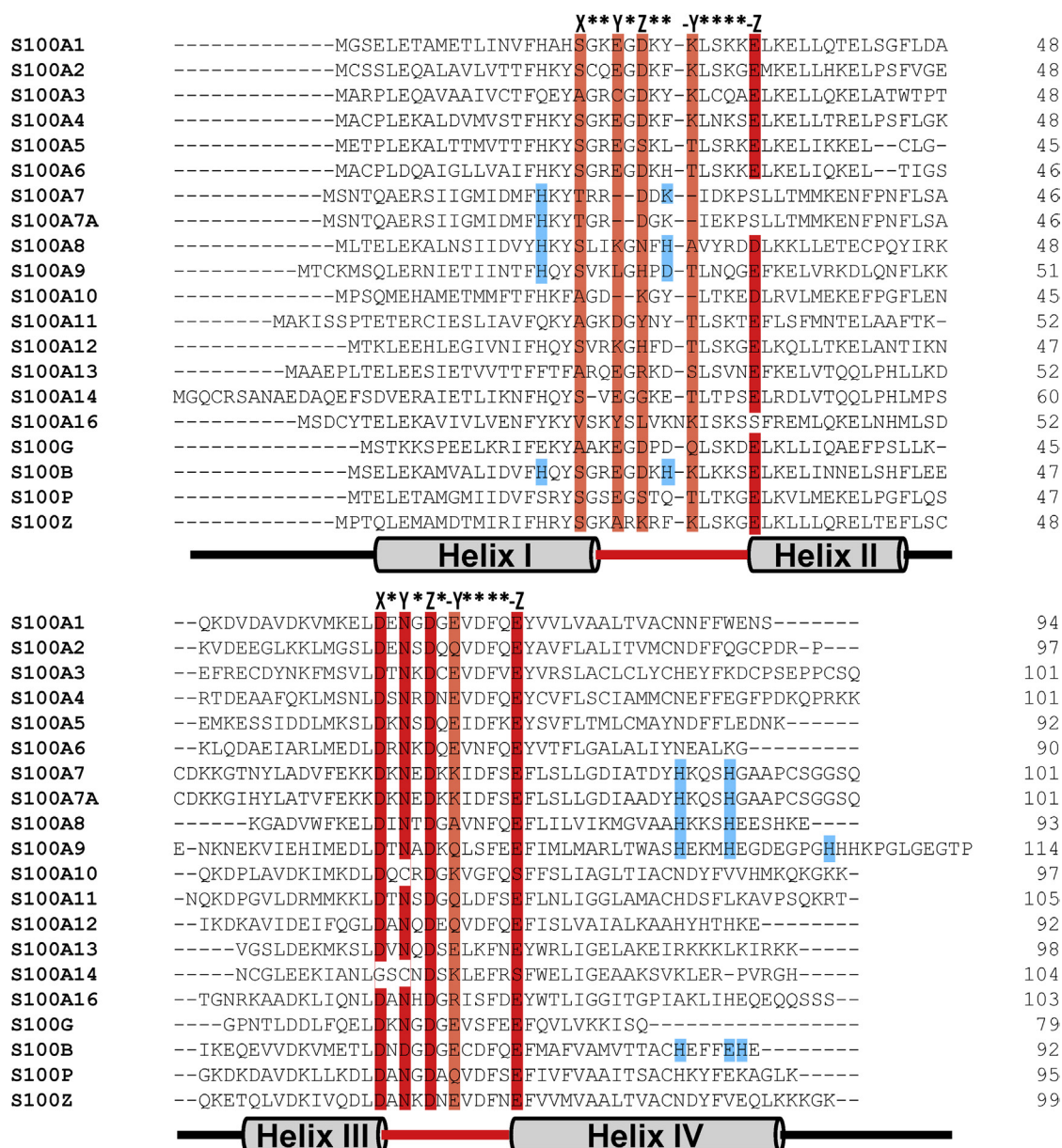
Some abbreviations are listed at the end of the chapter.

## STRUCTURAL DIVERSITY OF S100 MONOMERS AND MULTIMERS

### S100 Structure and Folding

S100 proteins are rather small proteins with a length of 79 to 114 amino acid residues corresponding to a size of 9 to 14 kDa [1,15,16]. Their sequence identities range from 22% to 57%, showing that the diversity within the family is quite large (Fig. 18.1) [1]. Under physiologic conditions most S100 proteins form multimers ranging from dimers to

decamers (Fig. 18.2) [17–19]. Low salt concentrations stabilize monomers which retain the native fold [20]. The basic structure of the different S100 protein monomers is very similar. Each monomer comprises two adjacent EF-hands connected by a flexible linker (Fig. 18.2A). The N-terminal EF-hand, composed of helices I and II, is specific for S100 proteins whereas the C-terminal EF-hand, involving helices III and IV, shows the classic architecture present in all other EF-hand proteins. Dimerization of S100 proteins occurs via helices I and IV from both monomers, forming a stable four-helix bundle. Helices II



and III of both monomers reside on each side of the dimer. These dimers serve as building blocks for the formation of larger multimeric assemblies such as tetramers, hexamers, octamers or even decamers (Fig. 18.2B–F). Most of these assemblies are homo-multimers. However, several S100 proteins form hetero-multimers as well, such as e.g. S100A8 with S100A9, S100B with S100A1 or S100A6 or S100A11 [21]. Multimerization is very often triggered by  $\text{Ca}^{2+}$  or  $\text{Zn}^{2+}$  binding, as in the case of S100A8/A9 heterotetramer formation (Fig. 18.2C) [19,22] or of S100A12 hexamerization (Fig. 18.2D), where both metal ions play a crucial role [23].

### $\text{Ca}^{2+}$ and Other Metal-Binding Properties

Many S100 proteins act as  $\text{Ca}^{2+}$  sensors, translating changing intracellular  $\text{Ca}^{2+}$  concentrations into a signal. In the

inactive  $\text{Ca}^{2+}$ -free state, the N-terminal EF-hand harbors a  $\text{Na}^+$  ion that is replaced by  $\text{Ca}^{2+}$  when  $\text{Ca}^{2+}$  levels rise beyond a certain threshold [24,25]. In this EF-hand,  $\text{Ca}^{2+}$  is coordinated mainly by backbone carbonyls and exhibits lower  $\text{Ca}^{2+}$  affinity than the classic C-terminal EF-hand, where  $\text{Ca}^{2+}$  is mainly coordinated by side chains from aspartate, asparagine and glutamate residues [16]. Mutation of one of these side chains results in the loss of  $\text{Ca}^{2+}$  binding as observed e.g. in S100A10.  $\text{Ca}^{2+}$  binding to S100 proteins triggers a large conformational change, opening the structure by a 90° degree movement of helix III [26]. The hydrophobic target interaction site that is exposed by the conformational change is mainly formed by residues from helix IV and the linker region [15].

Many S100 proteins bind  $\text{Zn}^{2+}$  with high affinity at sites distinct from the  $\text{Ca}^{2+}$  ones. The  $\text{Zn}^{2+}$ -binding S100 proteins can be divided into two groups. In the first group,

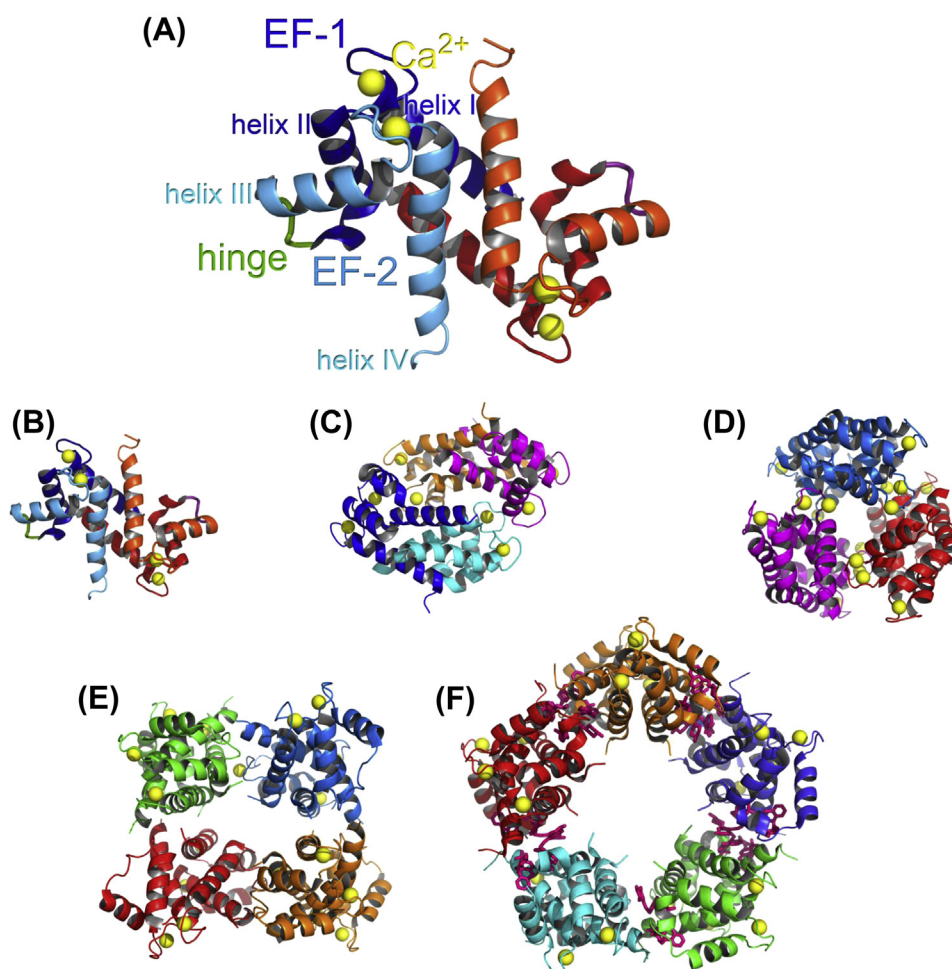


**FIGURE 18.2** Different multimeric assemblies of S100 proteins. (A) S100A4 dimer. The structure of  $\text{Ca}^{2+}$ -bound S100A4 (pdb code 3C1V) exhibits the typical dimeric assembly observed for many S100 proteins. The subunits are shown in red and blue, respectively. The N-terminal S100-specific EF-hand formed by helices I and II is shown in dark colors at the back of the molecule; the C-terminal canonical EF-hand encompassing helices III and IV is shown in bright colors in the front. Bound  $\text{Ca}^{2+}$  ions are shown as yellow spheres. (B) Same as A, but scaled to match the other multimeric S100 proteins. (C) The S100A8/A9 heterotetramer (pdb code 1XK4) is formed by two heterodimers. (D) S100A12 hexamer (pdb code 1GQM), composed of three S100A12 homodimers. (E). The S100B octamer (pdb code 2H61) is formed by four S100B homodimers. (F) A S100A4 decamer (pdb code 3KO0) that is assembled from five homodimers. The formation of this pentamer of dimers is triggered by phenothiazine, shown as magenta sticks.

**TABLE 18.1** Influence of Metal Ions on the Oligomeric State and Function of Some S100 Proteins

S100 Protein	Oligomerization State	Is Oligomerization Metal-Dependent?	Function	Reference
S100B	Dimer	No	Binds RAGE	18
	Tetramer	No	Binds RAGE with higher affinity	
	Hexamer/octamer	Ca <sup>2+</sup>		
S100A12	Dimer	No	Binds RAGE	43
	Hexamer	Ca <sup>2+</sup>	Binds RAGE with higher affinity	
S100A4	Multimeric	No	Neurite outgrowth	45
S100A8/A9	Heterodimer	No		46
	Heterotetramer	Ca <sup>2+</sup>	Microtubule formation	
S100A2	Dimer	No	Tumor suppressor	47
	Tetramer	Zn <sup>2+</sup>		29

comprising S100A2, S100A3 and S100A6, coordination of Zn<sup>2+</sup> involves predominantly cysteine residues [27–30]. In the second group, histidine, glutamate or aspartate residues bind Zn<sup>2+</sup> ions; this group includes S100A7, S100A7A, S100A8, S100A9, S100A12 and S100B. Interestingly, Zn<sup>2+</sup> binding to S100A12 or S100B increases the affinity of the proteins towards Ca<sup>2+</sup> by up to 1500-fold [31–33]. Moreover, in the presence of Zn<sup>2+</sup> the affinities of S100A9 and S100A12 towards their receptors RAGE or TLR4 increase by several hundred-fold [23,34], revealing a further regulatory function of Zn<sup>2+</sup>.

Cu<sup>2+</sup> binding has been reported for S100B, S100A12 and S100A13 [35–38]. However, the *in vivo* free Cu<sup>2+</sup> concentrations are rather low, raising the question of the physiologic role of the Cu<sup>2+</sup> binding observed *in vitro*. Recently, high-affinity binding of Mn<sup>2+</sup> has been observed for S100A8/A9 and revealed a new function of this protein [39]. As a part of the innate immune response, S100A8/A9 is released in high concentration at places of pathogenic invasion where it limits the availability of trace metal ions essential for microbial growth. Binding of Mn<sup>2+</sup> effectively inhibits the growth of pathogens and weakens their defense towards reactive oxygen species [40].

## S100 OLIGOMERS, AGGREGATES AND AMYLOIDS

### S100 Functional Oligomers

Multimer formation most likely regulates the activity and modifies the function of S100 proteins (Fig. 18.2). For multimerization – as well as for conformational changes and

stabilization – metal ions such as Ca<sup>2+</sup> and Zn<sup>2+</sup> have an important role (Table 18.1) [13]. For example, S100B forms larger oligomeric species such as tetramers, hexamers and octamers (Fig. 18.2E). The formation of the two largest multimers is enhanced by Ca<sup>2+</sup> binding, while the addition of EDTA eliminates these assemblies [18]. The multimers represent a large portion of S100B in human brain but the most stable is the tetramer, which does not dissociate into dimers [18]. Binding of dimeric and tetrameric S100B to RAGE is strictly Ca<sup>2+</sup> dependent. However, tetramers bind RAGE with higher affinity and promote cell survival whereas dimeric S100B binds with lower affinity and triggers a pro-apoptotic response [18].

S100A12 also requires Ca<sup>2+</sup> for interacting with its targets, including RAGE. The RAGE–S100A12 interaction mediates a pro-inflammatory response to cellular stress and can contribute to the development of inflammatory lesions [41,42]. As for S100B, the S100A12 hexamer is formed in a Ca<sup>2+</sup>-dependent manner (Fig. 18.2D) and has enhanced binding affinity to RAGE [43]. Another recent example is S100A4, where a specific inhibitor induces the formation of a homodecamer (Fig. 18.2F) which cannot bind target proteins any more, indicating that multimer formation is a potent modulator of S100 protein activity [44]. In addition, extracellular S100A4 oligomers are potent promoters of neurite outgrowth and survival [45]. Finally, the Ca<sup>2+</sup>-induced S100A8/A9 heterotetramer (Fig. 18.2C) controls microtubule formation [46].

Apart from Ca<sup>2+</sup>, Zn<sup>2+</sup> was also reported to influence the degree of oligomerization of S100A2. The binding of Zn<sup>2+</sup> to its lowest affinity binding site induces the formation of an S100A2 tetramer via the assembly of two homodimers, whereby the metal is coordinated by a cysteine from

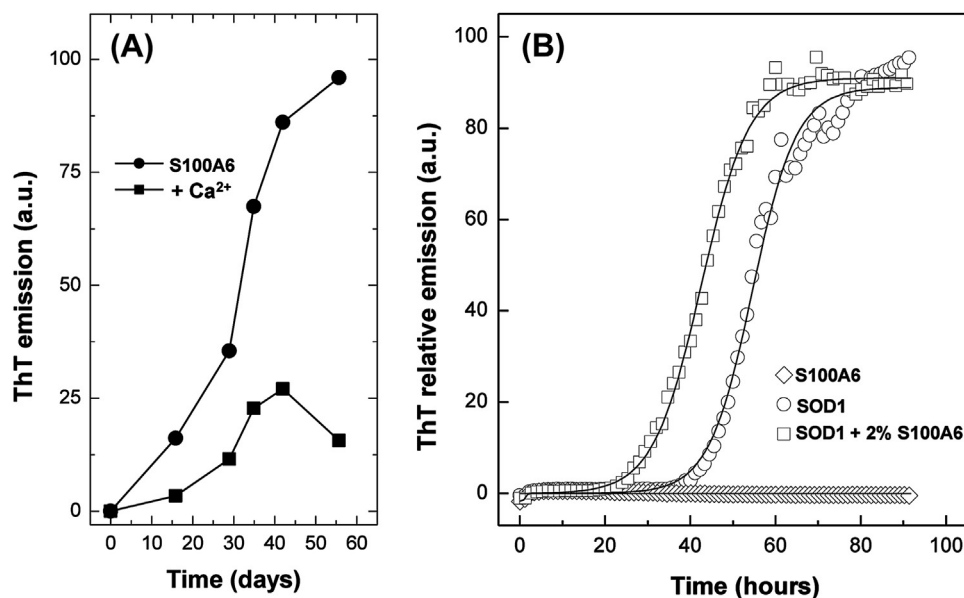


**FIGURE 18.3** Amyloidogenesis kinetics of S100A6. Amyloid formation kinetics as assessed by the ThT binding assay. (A) Amyloid formation for apo (●) and Ca<sup>2+</sup>-S100A6 (■) at pH 7, 37°C, 3 mg·ml<sup>-1</sup> and 1000 rpm. Ca<sup>2+</sup> partially inhibits amyloid formation. (B) SOD1-S100A6 amyloid cross seeding. SOD1 aggregation (pH 7, 37°C, 50 μM SOD1 and 600 rpm) was monitored for SOD1 alone (○) and in the presence of 2% native apo S100A6 (□). The aggregation lag phase is shortened (from 45 h to 31 h) in the presence of S100A6. All the ThT signal is due solely to SOD1 aggregation as S100A6 alone has a negligible contribution (◇). Adapted from reference 14.

each subunit [29]. Metal ions thus play an important role in the formation of functional S100 oligomers, and recent observations on S100A8/A9 [12,13] suggest that they may also be involved in the formation of oligomeric and fibrillar assemblies.

### Amyloidogenic and Aggregation Potential of S100 Proteins

Some members of the S100 protein family possess an inherent potential to form amyloid fibrils. Despite the fact that several factors influence the amyloidogenic process, the primary sequence – to a large extent – defines the aggregation and fibrillation propensity of a polypeptide chain. This potential can be estimated through different computational algorithms, e.g. Zyggregator, that estimates the aggregation propensity [48], and Waltz, which is able to identify amyloid-forming regions in functional amyloids [49]. Indeed, the intrinsic aggregation propensity scores of the monomeric forms of S100A8 and S100A9 at pH 2.5 and 7.0 were determined to be of the same order of magnitude as that of the Aβ peptide, which forms amyloid deposits in Alzheimer's disease [12]. Taking into account that S100 proteins have a similar chemical and structural identity, it was hypothesized that the ability to form amyloid structures could be a generalized property among the S100 protein family. When other S100 proteins, including S100A3, S100A6, S100A12 and S100B, were tested for the formation of amyloid-like structures at pH 2.5 and 57°C, it was found that most of them formed thioflavin-T (ThT)-binding

amyloid structures, with S100A12 being the only exception. The formation of both amyloid fibrils and other precursor structures was confirmed by atomic force microscopy (AFM) [13].

### Effects of S100 on Aggregation Cross-Seeding

Although several S100 proteins aggregate into amyloid-like structures, some of them have the ability to modify or enhance the aggregation potential of other proteins. An example is S100A6, an amyloidogenic protein that aggregates into fibrils under physiologic conditions and is capable of enhancing the aggregation of SOD1 [14]. Both proteins are involved in amyotrophic lateral sclerosis (ALS), a fatal neurodegenerative disorder [50]. The Zyggregator algorithm predicts a high propensity for the formation of amyloid-like structures by S100A6 [14]. In fact, at acidic conditions and high temperature (pH 2.5 and 57°C) the ThT binding kinetics revealed a fast fibril formation process with no lag phase. The formation of aggregates and fibrils was also observed through transmission electron microscopy (TEM). Interestingly, Ca<sup>2+</sup> produced an inhibitory effect on the aggregation kinetics, probably because this metal ion promotes anti-parallel β-sheet conformations that can repress fibrillation. Under physiologic conditions (pH 7.0 and 37°C) this protein also forms amyloid-like fibrils in a slower process, but without a lag phase (Fig. 18.3A). The formation of S100A6 amyloidogenic structures lead us to hypothesize a new role for S100 proteins in brain damage. S100A6 is overexpressed in astrocytes which are associated

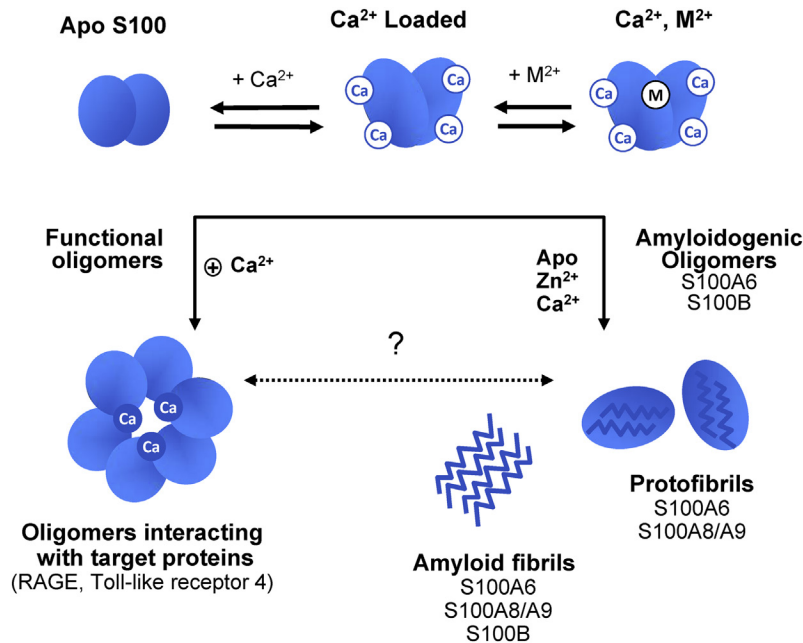


**FIGURE 18.4** Metal ion-induced conformational and oligomerization changes in S100 proteins. Native S100 proteins can bind  $\text{Ca}^{2+}$  and undergo the characteristic structural opening involving mainly helix III.  $\text{Zn}^{2+}$  or other metal ions ( $\text{M}^{2+}$ ) can bind to some S100 proteins at sites distinct from the  $\text{Ca}^{2+}$  ones and mediate specific conformational or stability changes as well as oligomerization and aggregation pathways. Each conformational state is associated with specific signaling properties or pathology. Adapted from reference 13.

with degenerating motor neurons in ALS patients. In these neurons, SOD1-enriched inclusions were also found [51], rendering the amyloid cross-seeding between the two proteins a real possibility under *in vivo* conditions [52]. Botelho et al showed that native S100A6 nucleates SOD1 fibrillation, leading to a decrease in the lag phase by more than 10 h (Fig. 18.3B), thus suggesting a novel role for S100A6 aggregation in human neuropathologies [14].

The pro-inflammatory protein S100A9 was also shown to interact with the  $\text{A}\beta_{1-40}$  peptide, inducing its fibrillation [53]. Co-incubation of S100A9 and  $\text{A}\beta_{1-40}$  at physiologic conditions (pH 7.4 and  $37^\circ\text{C}$ ) produced massive fibrillar aggregates observed by AFM. The interaction of these two proteins was also observed through the kinetics of amyloid formation (ThT-binding assay) and transitions in secondary structure (far-UV circular dichroism). Interestingly, the addition of  $\text{A}\beta_{1-40}$  inhibits S100A9 cytotoxicity. This may occur via the binding of toxic S100A9 species to  $\text{A}\beta_{1-40}$  amyloid structures. Altogether, these results suggest that S100A9 secretion during inflammation leads to the formation of amyloid plaques. This can nevertheless be a protective mechanism against  $\text{A}\beta$ -associated toxicity in Alzheimer's brains.

### Role of Metal Ions in Aggregation Pathways

The binding of different metal ions to S100 proteins may modulate their conformation, folding and – ultimately – function. As discussed above, the identification of high

amyloidogenic potential in S100 proteins suggests that they may have the ability to acquire amyloid-like conformations under certain physiologic conditions, and it becomes clear that metal ions can have an important role in this process (Fig. 18.4) [13]. The general role of metal ions as modulators of protein conformation, misfolding and aggregation in disease has been recently reviewed [52].

In the case of S100A2, binding of  $\text{Ca}^{2+}$  and  $\text{Zn}^{2+}$  promotes conformational changes that alter protein stability:  $\text{Ca}^{2+}$  has a stabilizer role whereas  $\text{Zn}^{2+}$  has the opposite effect [54]. These metal ions also have an impact on the formation of functional oligomers, as in the case of the  $\text{Ca}^{2+}$ -dependent S100B hexa- and octamerization [18].  $\text{Ca}^{2+}$  and  $\text{Zn}^{2+}$  also play a determinant role in promoting amyloid assembly of S100A8/A9 proteins *in vivo* [12]. Besides the above mentioned factors, metal ion dyshomeostasis or anomalous protein–metal interactions can also influence S100 functional states within a physiologic context, leading to the formation of amyloid structures or precursor oligomers [52].

## BIOIMAGING OF S100 AMYLOIDS BY AFM AND TEM

### Techniques to Study Protein Amyloid Formation

Protein polymerization and aggregation *in vivo* and *in vitro* is far from being understood, and numerous techniques

have been developed in order to unravel the underlying mechanism with the ultimate aim of understanding the respective pathologies and establishing inhibition strategies and therapeutic approaches. X-ray diffraction techniques, solid-state magic-angle spinning NMR spectroscopy, circular dichroism spectroscopy and microscopy studies, among others, have been utilized to detect and examine the chemical, electronic, material and structural properties of amyloid fibrils at up to Ångström spatial resolution [55]. Nevertheless, imaging amyloid morphology at the ultrastructural level is still a challenge and remains a goal of researchers.

Both AFM and TEM microscopies play a key role in studies on the morphology and pathways of amyloid assembly. Typical amyloid fibrils are characterized by a nanometer size in cross-sectional dimensions and can reach up to micrometer length and longer in their axial growth, which makes them a perfect object for these microscopy techniques [56–58], while being far too small for optical microscopy. AFM and TEM provide sub-nanometer and even up to Ångström (AFM in z-axis) resolution and at the same time can image micrometer size structures. This over 1000-fold dynamic range surpasses the optical diffraction limit attainable by optical microscopes and provides insights into sub-molecular details comparable with high-resolution molecular structural techniques. AFM does not require any special treatment of the samples and is able to image them in air or liquid. For TEM studies, biologic macromolecules, due to their low density and therefore contrast, are subjected to negative staining, rotary shadowing and cryo-EM [56].

Both TEM and AFM have been widely used for imaging a variety of materials, ranging from carbon nanotubes [59] to human tissues, and they constitute a powerful tool that even allows atomic resolution. Amyloid fibrils of different origins have also been imaged *in vivo*, *ex vivo* and *in vitro* by both AFM and TEM. Compared to other techniques, TEM and AFM usage is more widespread, easier to access and handle, and has been used to characterize various assembly states of A $\beta$ ,  $\alpha$ -synuclein, IAPP, TTR and lysozyme, among others [12,57,60–65].

### Sources of Amyloid – *In Vivo* and *In Vitro*

*In vivo* imaging of amyloids by microscopy techniques in affected tissues is limited by the available tissue sources and cannot provide information on the dynamics of fibril formation. Most studies are based on observations using extracted amyloids and fibrils produced *in vitro*. *In vitro* fibril production has been a powerful tool for studying the mechanisms leading to amyloid formation. Theories for the events occurring *in vivo* have been proposed based on *in vitro* results. Virtually all types of fibril were produced *in vitro* from their native precursors, suggesting that the amyloidogenic potential is a feature shared by all polypeptide chains [66]. For *in vitro* studies, amyloid fibrils are generated in

solution or suspension and then captured on mica in air or buffer (for AFM studies) or on a rapidly prepared TEM grid. Much evidence has been accumulated showing that synthetic fibrils are morphologically similar to those formed *in vivo*, indicative of a predominant role for the amyloidogenic potential of proteins in amyloid disorders.

Fibril formation *in vitro* also opened the possibility of studying the process by which a native soluble protein loses its normal fold and aggregates into fibrils, paving the way for a better understanding of the mechanism that culminates in amyloid formation and the design of drugs that interfere with such a process. Protein denaturation and the amyloidogenic pathway involve the formation of several intermediates with variable quaternary, tertiary and secondary structures. Accordingly, several amyloidogenic intermediate species *en route* to mature amyloids have been identified in different amyloidotic disorders. Furthermore, fibril formation is dependent on factors such as pH, protein concentration, time and metal ions. Here we describe highly heterogeneous S100 protein aggregates visualized by microscopy techniques and occurring both *in vitro* (under different pH, Ca<sup>2+</sup> and other salt concentrations) and extracted from *ex vivo* tissue.

### S100A8/A9 Amyloids

The first proteins in the S100 family that were found to be amyloidogenic were S100A8/A9 [12]. Indeed, the overall aggregation scores for S100A8 calculated using intrinsic propensities for the aggregation of individual amino acids are comparable to those of A $\beta$  [12,67]. In agreement, amyloid structures of S100A8/A9 were formed *in vitro* from proteins extracted from granulocytes (and produced recombinantly in *Escherichia coli*) which were incubated at pH 7.4, 37°C with agitation, or pH 2.0, 57°C without agitation. Under both conditions, S100A8/A9 were found to assemble into heterogeneous fibrillar species as illustrated in Figure 18.5. At pH 7.4, oligomeric species and short protofilaments were observed after 2 weeks of incubation (Fig. 18.5A), while upon further incubation, for up to 8 weeks, thick fibrillar bundles of a few micrometers in length were massively populated (Fig. 18.5B,C). Their dimensions were estimated in AFM cross-sectional analysis by measuring z-height, the most accurate AFM parameter. The height of fibrillar bundles reached ca. 15–20 nm, while the height of individual filamentous structures was ca. 5 nm (Fig. 18.5G,H). Fibrillar lateral assembly and thickening may be a contributing factor to their stability and resistance to different environmental factors and proteases, when they spontaneously assemble *in vitro* or *in vivo*.

In the S100A8/A9 samples incubated at pH 2.0 without agitation, the spherical oligomeric species and protofilaments were also formed in ca. 2 weeks (not shown).

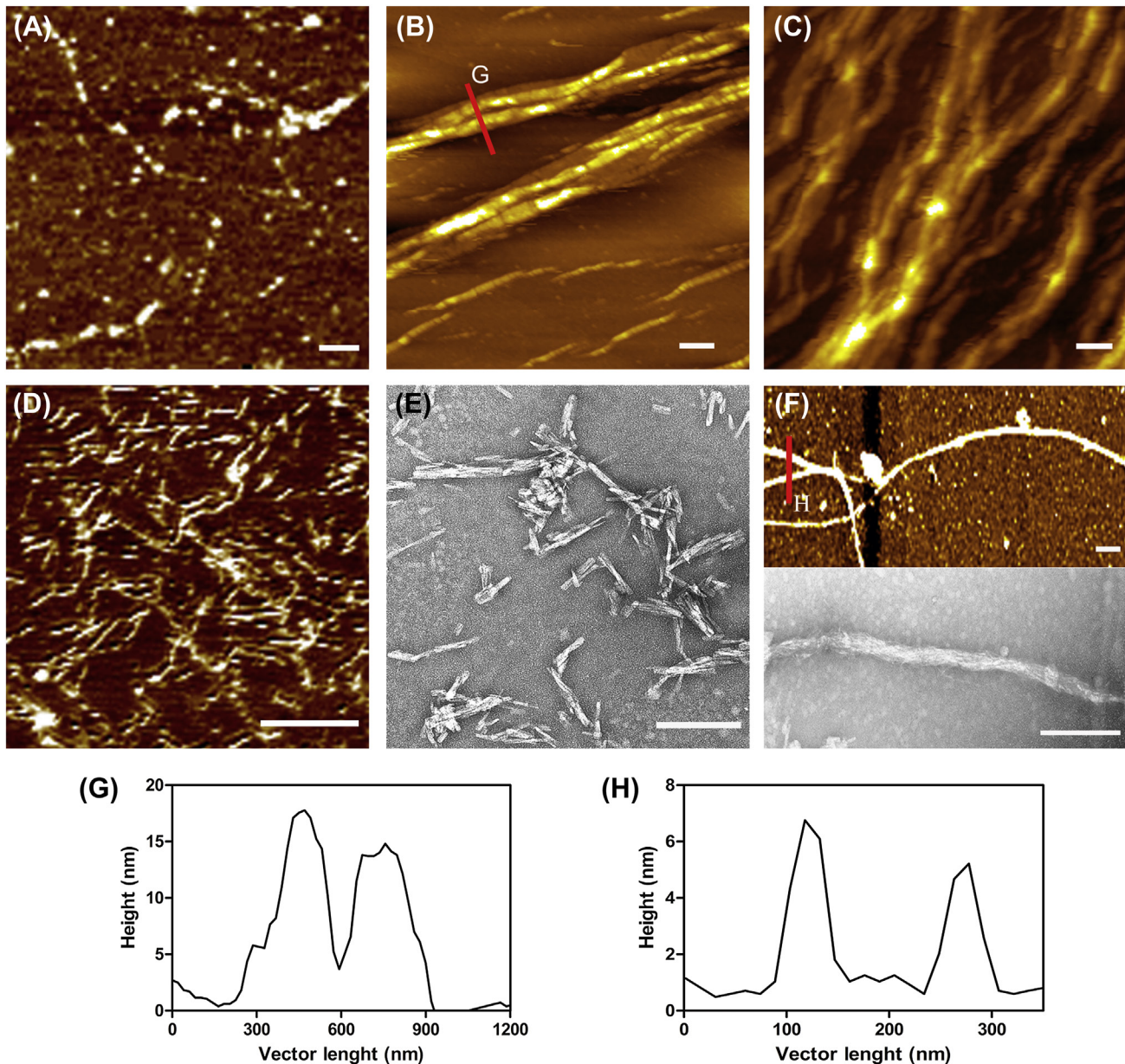


**FIGURE 18.5** AFM and TEM imaging of S100A8/A9 amyloids produced *in vitro*. AFM height images of (A) oligomers produced at pH 7.4, 37°C with agitation after 2 weeks and (B,C) fibrillar bundles formed after 8 weeks of incubation. (D) AFM height and (E) TEM images of heterogeneous amyloid fibrils produced at pH 2.0 and 57 °C after 4 weeks of incubation without agitation, and (F) some larger scale suprafibrillar bundles observed in the same samples by AFM (top) and TEM imaging (bottom). All samples contain residual  $\text{Ca}^{2+}$  and  $\text{Zn}^{2+}$  ions. (G,H) AFM cross-sections of amyloid structures at the positions indicated by red lines and corresponding white letters in panels B and F. Scale bars: 250 nm.

After 4 weeks, short straight fibrils of sub-micrometer length were highly populated, as observed very consistently by both AFM and TEM imaging (Fig 18.5D,E). They coexisted together with long filamentous structures from a few hundred nanometers to micrometer scale lengths, which were also observed by both AFM and TEM (Fig. 18.5F). The height of representative structures in AFM cross-section was ca. 4–5 nm (Fig. 18.5H).

### Amyloidogenic Properties of S100A6 Studied by TEM

The association of S100 proteins – namely, their aggregated states – with human disease has been recently expanded by the description of S100A6 as an amyloidogenic protein and its seeding effect towards SOD1 amyloidogenesis, characteristic of ALS [14]. The importance of this finding was two-fold: on the one hand, it suggested

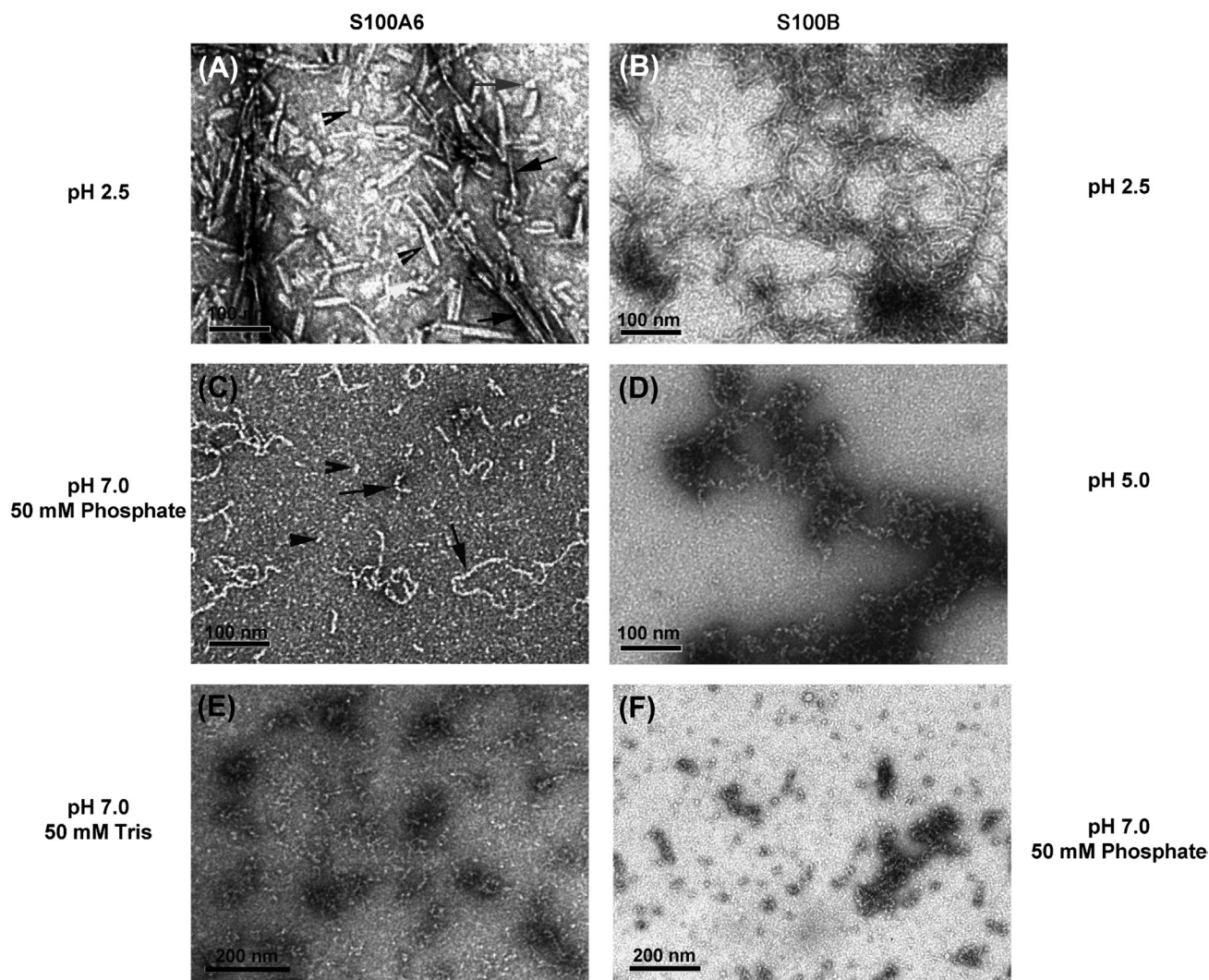


**FIGURE 18.6** Effect of pH and buffer conditions in S100A6 and S100B fibril formation. (A) S100A6 fibrils assembled at glycine pH 2.5 for 28 days are polymorphic in nature, presenting 4–5 nm wide fibrils, isolated or laterally assembled in thicker fibrils (A, black arrows) and 15 nm wide fibrils of variable length (A, black arrowhead). Other structures resembling oligomers are also visualized (A, gray arrow). (C) Increasing pH to 7.0 in phosphate buffer results in single 8 nm wide fibril species distinct from the ones obtained at lower pH. (E) At pH 7.0 and Tris 50 mM, the process of fibril formation is delayed as only amorphous aggregates and pre-fibrillar material are detected. S100B also forms fibrils, but to a lower extent. (B) At pH 2.5, fibrils are generated abundantly but the morphology is closer to that of S100A6 fibrils at pH 7.0 in phosphate buffer. (D) A similar situation occurs at pH 5.0 acetate. (F) At neutral pH, S100B does not form fibrils and only intermediate species are observed, at least during 28 days incubation at 37°C.

novel mechanisms in ALS etiology; on the other hand, it pointed to widespread amyloidogenic potential in the S100 family, with as yet unknown relevance. For this reason, the high-resolution characterization of these novel amyloids and the corresponding aggregation pathways is invaluable. S100A6 forms typical amyloid fibrils under acidification (Fig. 18.6A,C,E). As reported for other amyloidogenic proteins [61–63], the fibrils are polymorphic, exhibiting different species [14]. It is noteworthy that there are fibrils of 4–5 nm diameter, isolated or laterally assembled into thicker fibrils (Fig. 18.6A, black arrows) and 15 nm wide fibrils of variable length (Fig. 18.6A, arrowheads). Other

structures resembling oligomers were also visualized (Fig. 18.6A, gray arrow). Interestingly, coiled fibrils were not observed, although additional analyses, such as metal shadowing followed by TEM, are necessary to completely rule out the presence of this feature. Besides the differences in diameter, it is also interesting to note the presence of long thin fibrils and shorter thicker fibrils. This may be representative of distinct aggregation mechanisms, occurring at least *in vitro*. Accordingly, the long thin fibrils of 4–5 nm diameter correspond to elementary protofilaments formed by vertical stacking of the basic unit, e.g. the S100 monomer [13]. These protofilaments can

associate with each other and form higher-order structures, constituting mature fibrils. Alternatively, the later can be formed by longitudinal growth of full-width species, justifying the presence of thicker but shorter fibrils. Indeed, this pathway might also apply to the formation of S100A6 fibrils because thick, but short, structures were observed. Whether these two distinct mechanisms exist *in vivo* is not known, but they may represent a modulation of S100 fibril formation, with different impacts on cellular toxicity and disease development.

At pH 7.0 (50 mM phosphate), S100A6 fibrils were still formed, although less abundantly than at pH 2.5 (Fig. 18.6C). Interestingly, increasing pH also rendered the fibrils' population more homogenous, especially concerning the diameter, as only approximately 8 nm wide fibrils were observed. The 8 nm wide fibril is also reported as the most prominent species for other amyloid fibrils generated *in vitro*, such as TTR [61]. Nevertheless, it is still possible to detect fibrils of variable length and, occasionally, small oligomers (Fig. 18.6C, arrowheads). In this case, fibrils seem to form upon stacking of these spherical oligomeric species (Fig. 18.6C, arrows). The higher-order thicker fibrils are not observed under these conditions. The observation that S100A6 aggregates differently at pH 7.0 when using 50 mM tris indicates that salt concentration and ions also play an important role in the aggregation process. In this case, the fibril formation process appears to be delayed as mainly aggregates and pre-fibrillar material were detected (Fig. 18.6E).

### S100B Amyloid Formation *In Vitro*

Similarly to S100A6, S100B enters different aggregation pathways at different pH values. However, the morphology of – the much more abundant – S100B fibrils generated at pH 2.5 (50 mM glycine, Fig. 18.6B) is closer to that of S100A6 fibrils at pH 7.0 (Fig. 18.6E). (In fact, increasing the pH to 5.0 and 7.0 does not result in fibril formation, as observed for S100A6, but instead leads to the formation of intermediate species, such as large amorphous aggregates and oligomers of different sizes and shapes, as those depicted in Fig. 18.6D and Fig. 18.6F, respectively). In this regard, the S100B behavior at pH 7.0 in 50 mM phosphate is closer to the behavior of S100A6 in tris buffer, indicating a slower kinetics and suggesting a lower amyloidogenic potential.

The kinetics of S100A6 and S100B fibril formation is slow when compared to that of other amyloidogenic polypeptides, such as amylin and A $\beta$  [68,69] or even other proteins with slow assembly rates, such as TTR [61]. Upon 33 days of incubation of S100A6 at 37°C, TEM showed only the formation of aggregates and oligomers (Fig. 18.7A). Even after 65 days, the presence of fibrils was scarce (Fig. 18.7B) and aggregates and oligomers were still observed abundantly.

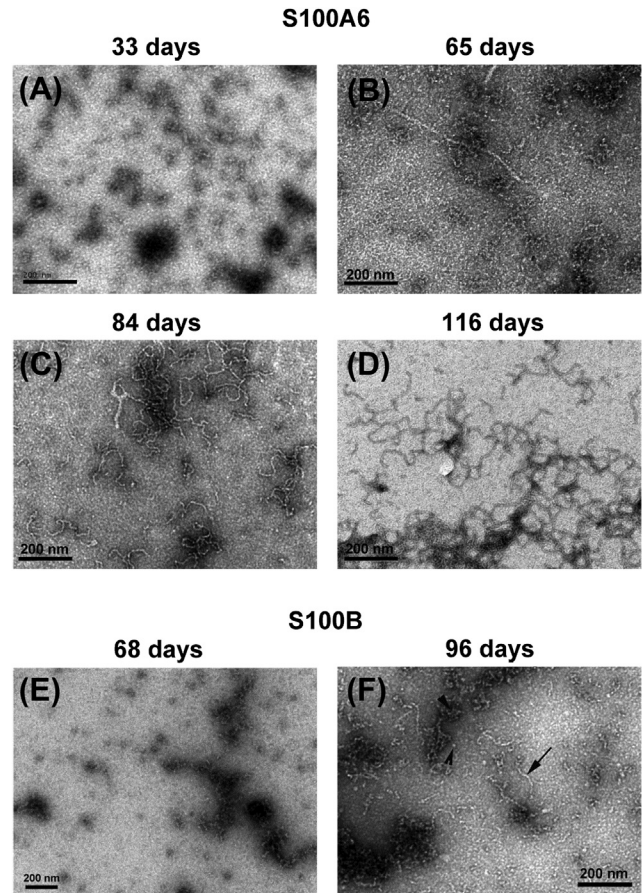


**FIGURE 18.7** Effect of incubation time on S100A6 and S100B fibril formation at neutral pH. S100A6 fibril formation initiates with the assembly of aggregates and oligomers (A) which organize into 8–10 nm wide fibrils after extended incubation at 37°C (B, C). (D) The process is accompanied by fibril elongation whereas no fibril diameter changes are detected, culminating in fibril bundling along with additional intertwining and tangling. S100B shows a similar yet slower behavior. (E,F) Aggregates and oligomers are present throughout the time course of incubation and are still visible after 96 days at 37°C.

Long incubation times, such as 84 days at 37°C, result in the production of homogenous fibril preparations (Fig. 18.7C). These fibrils were variable in length but very homogenous in diameter (8–10 nm). An exhaustive sample visualization also permitted the detection of spherical species, resembling either the monomeric protein or small oligomers about 6–7 nm in diameter. Further incubation over time resulted mainly in increased length whereas no alterations were visualized regarding fibril diameter (Fig. 18.7D).

S100B shows a similar behavior, and thus the mechanism of fibril formation seems to involve the rearrangement of aggregates and oligomers (Fig. 18.7E) into distinct fibrils (Fig. 18.7F, arrow). Again, kinetics is slower than for S100A6, and after prolonged incubation at 37°C large aggregates and oligomers were also abundantly visualized, despite fibrils being present in generous amounts, (Fig. 18.7F, arrowheads).

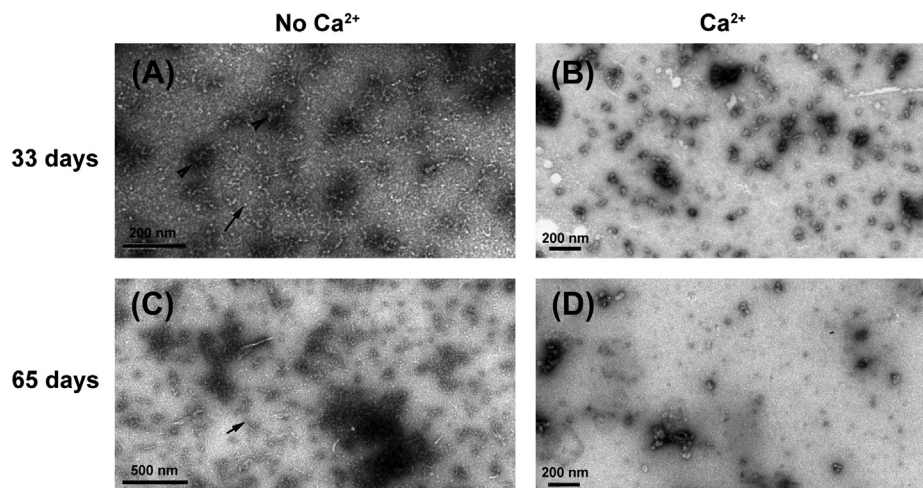


**FIGURE 18.8** Effect of  $\text{Ca}^{2+}$  in S100A6 fibril formation. (B, D)  $\text{Ca}^{2+}$  affects S100A6 fibrillogenesis, preventing fibril formation by arresting an off-pathway oligomeric species, whereas (A, C) in the absence of  $\text{Ca}^{2+}$  large initial amorphous aggregates, small oligomers and short fibrils are produced. Samples were obtained at neutral pH.

As we have discussed above, S100 proteins are  $\text{Ca}^{2+}$ - and  $\text{Zn}^{2+}$ -binding proteins, and the study of metal-modulated aggregation propensity has just started. Recent data showed that  $\text{Ca}^{2+}$ , but not  $\text{Zn}^{2+}$ , represses S100A6 aggregation, resulting in antiparallel  $\beta$ -sheet conformations, indicative of oligomeric species structurally distinct from fibrils, as assessed by Fourier transform infrared spectroscopy [14]. TEM analysis provided new insights on the structures formed, confirming the presence of oligomers in the presence of  $\text{Ca}^{2+}$  (Fig. 18.8B,D). Additionally, TEM also shows that the nature of the oligomers formed in the presence of the ion are different from the ones present in preparations without  $\text{Ca}^{2+}$  (Fig. 18.8). This indicates that  $\text{Ca}^{2+}$  alters the aggregation pathway of S100A6, resulting in homogenous preparations of oligomers *versus* fibrils. Whereas in the absence of  $\text{Ca}^{2+}$  the predominant species are amorphous aggregates and small spherical oligomers (Fig. 18.8A,C, arrowheads and arrows, respectively), in the presence of  $\text{Ca}^{2+}$  aggregates are absent and oligomers are larger, probably representing off-pathway species (Fig. 18.8B,D). In fact, the species formed upon  $\text{Ca}^{2+}$  incubation are not toxic as assessed by viability assays in cellular models [14].  $\text{Ca}^{2+}$  also prevents the generation of fibrils, probably by stabilizing the off-pathway oligomer stage.

### Ex Vivo S100A8/A9 Amyloids Imaged by AFM and TEM

For the first time, amyloids of pro-inflammatory S100A8/A9 proteins formed *in vivo* were found in calcified deposits, extracted from the prostate, known as *corpora amylacea* [12]. These deposits were classified as local amyloid deposits associated with prostate gland inflammation and aging. Indeed, *corpora amylacea* are frequently observed

in the prostate when it undergoes structural remodeling due to age-dependent reduction in reproductive function. This may lead to benign prostatic hyperplasia, observed in 70% of men in their 60s, and even cancer. *Corpora amylacea* inclusions are often adjacent to damaged epithelium and focal inflammatory infiltrates. They can be triggered by inflammation and provide a feed-forward loop exacerbating further inflammation, infection and cancerogenesis [12]. There is growing evidence that inflammation plays a crucial role in prostate pathogenesis: it is associated with 40–90% of benign prostatic hyperplasia [70] and leads to 20% of all human cancers. We have found that protein deposits constitute up to 30% of *corpora amylacea* contents, the remainder being calcified inorganic compounds [12]. AFM and TEM analysis of extracts from *corpora amylacea* of seven patients subjected to prostatectomy due to cancer revealed a variety of highly heterogeneous molecular aggregates (Fig. 18.9). These included spherical oligomeric species of ca. 2–3 nm in height in AFM cross-sections (Fig. 18.9A), which closely resembled oligomeric precursors of amyloid fibrils described for numerous peptides and proteins [57,71]. In addition, extensive networks of typical fibrillar amyloids 4–8 nm in height and micrometers in length were imaged by AFM (Fig. 18.9B), and straight and rigid fibrils a few hundred nanometers in length were detected by TEM (Fig. 18.9C). There were also larger-scale supramolecular filamentous assemblies, reaching a few micrometers in length and up to ca. 500 nm in thickness (Fig. 18.9D), and large round aggregates of ca. 200–300 nm diameter at half-height and ca. 50–70 nm height in AFM cross-sections (Fig. 18.9E). Comparison of *in vitro* and *ex vivo* amyloids (Fig. 18.5 and 18.9) revealed their general similarity and also their tendency to assemble into large supramolecular complexes.

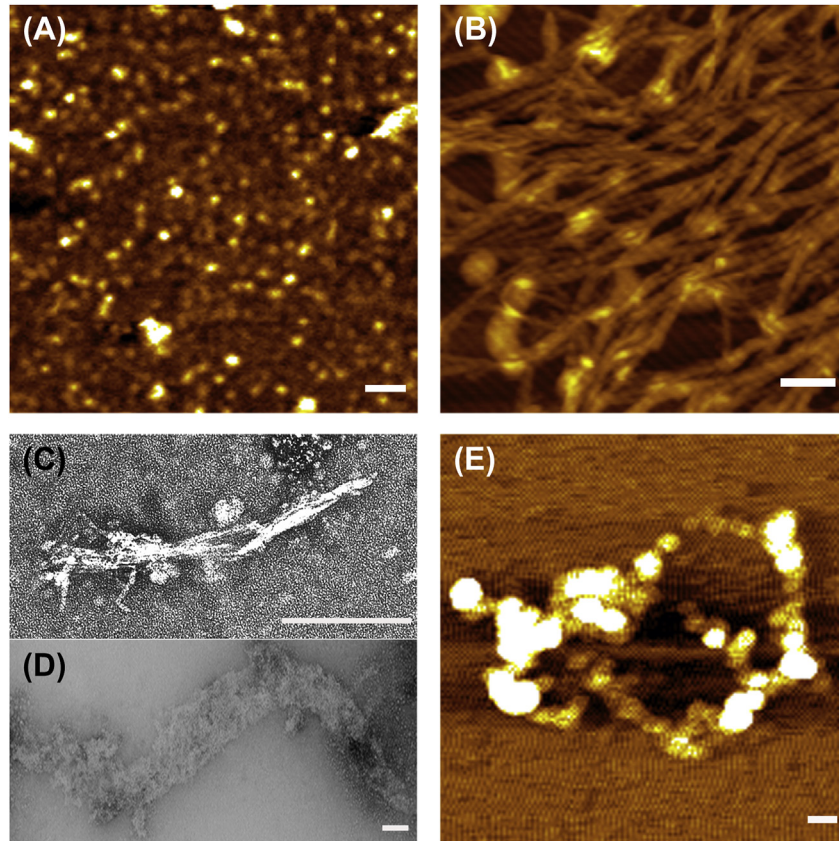


**FIGURE 18.9** AFM and TEM imaging of S100A8/A9 amyloids extracted from *ex vivo* prostate *corpora amylacea* deposits. AFM height images of (A) oligomers, (B) fibrillar networks. TEM images of (C) amyloid fibrils and (D) filamentous suprastructures. AFM height images of (E) round, particulate-type assemblies. Scale bars: 250 nm.

### Macroscopic Amyloid Properties of *Corpora Amylacea* Studied by Optical Microscopy

*Corpora amylacea* inclusions may grow up to millimeter scale, as shown in Figure 18.10A, and may be very heterogeneous in size [12]. In extreme cases, their bulk weight may constitute up to one third of the prostate gland. These inclusions were also characterized by typical amyloid features as observed in optical microscopy. Specifically, they bound the amyloid-specific fluorophore ThT, which presented increased fluorescence under the fluorescence microscope (Fig. 18.10B); the Congo Red dye, also used to identify amyloids, resulted in red staining and Congo Red green birefringence under polarized light, as observed in the optical microscope (Fig. 18.10C).

In immunohistochemical analyses, all *corpora amylacea* specimens were stained positively with antibodies recognizing an amyloid conformational epitope [72], S100A8 or S100A9 (Fig. 18.11). This indicates that the S100A8/A9 amyloid material constitutes a significant mass of *corpora amylacea*.

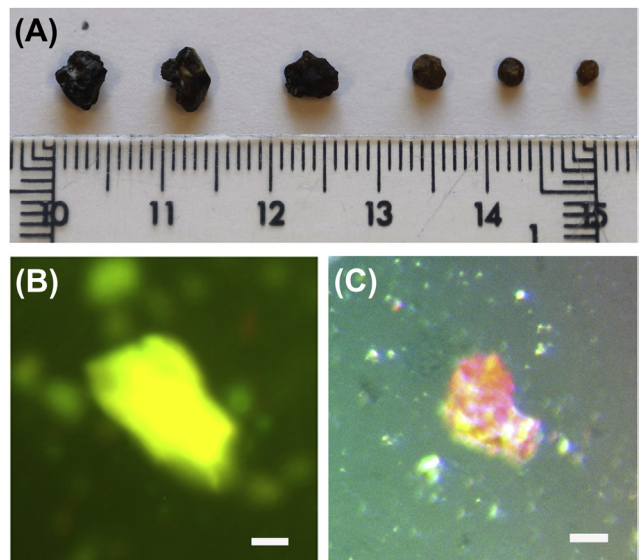


**FIGURE 18.10** Optical images of *corpora amylacea* deposits in the aging prostate. (A) Size of *corpora amylacea* deposits extracted as a result of prostatectomy compared to a ruler shown in centimeters. (B) ThT and (C) Congo Red staining of *corpora amylacea* observed in fluorescence and polarized optical microscopes, respectively. Scale bars: 25  $\mu$ m.

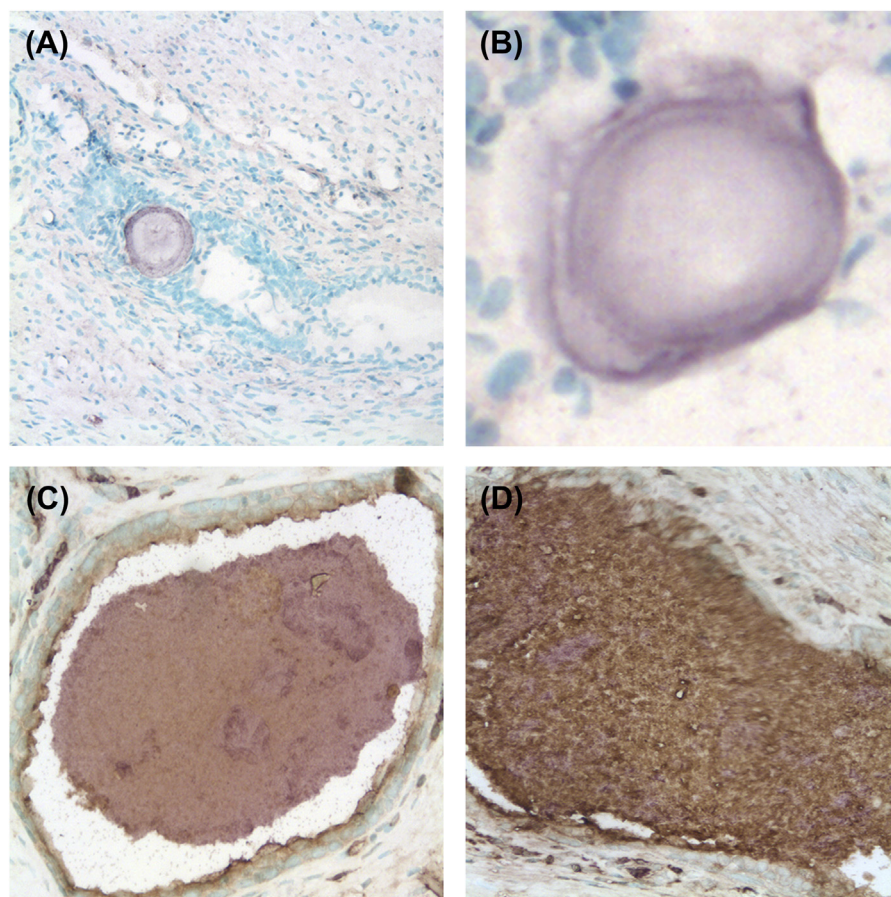


**FIGURE 18.11** Immunohistochemical staining and optical imaging of *corpora amylacea* deposits in the aging prostate. Immunostaining of *corpora amylacea* inclusions by generic antibodies to amyloid fibrils shown in purple at (A) with 100 $\times$  and (B) 200 $\times$  magnification, respectively. Co-immunostaining of *corpora amylacea* with anti-S100A8 (shown in purple) and anti-S100A9 IgG (shown in brown) at (C) with 200 $\times$  and (D) 400 $\times$  magnification, respectively.

## CONCLUSIONS

Above, we have demonstrated that microscopy techniques such as AFM and TEM are able to provide high-resolution insights into the pathways of amyloid assembly of S100 proteins and reveal the complex hierarchy of their amyloid species. S100 proteins are intrinsically amyloidogenic, and we may anticipate that more amyloids of these proteins will be discovered in coming years, both *in vitro* and *in vivo*. The direct involvement of pro-inflammatory S100A8/A9 proteins in the formation of *corpora amylacea* emphasizes the role of inflammation and amyloid formation in age-dependent prostate remodeling and cancerogenesis. As the enhanced level of S100 proteins in general is a characteristic feature of numerous inflammatory conditions, cancers and degenerative conditions taking place in different tissues and organs, they may also effectively contribute to pathology via amyloid depositions. The conformational plasticity of S100 proteins is modulated by  $\text{Ca}^{2+}$  and other metal ions, and the effect of various environmental factors on their amyloid

self-assembly requires thorough investigation. Learning how to regulate the conformational and aggregation properties of these proteins may be a key for effective therapeutic intervention in multiple disorders linked to S100 proteins.

## Abbreviations

AFM, atomic force microscopy; ALS, amyotrophic lateral sclerosis; RAGE, receptor for advanced glycation end-products; TEM, transmission electron microscopy; ThT, thioflavin-T; TLR4, toll-like receptor 4.

## ACKNOWLEDGMENTS

This work was supported in part by the Fundação para a Ciência e Tecnologia (FCT/MCTES, Portugal) through research grants PTDC/QUI/70101, PTDC/EBB-BIO/117793/2010, and PTDC/QUI-BIQ/117789/2010 (to CMG), doctoral fellowship SFRH/BD/31126/2006 (to HMB) and Research fellowship B017/BI-BI/2012 - PTDC/QUI-BIQ/117789/2010 (to SBC), and by the strategic Grant PEst-OE/EQB/LA0004/2011 (to the ITQB Laboratório Associado).

This work was also funded in part by a Terry Fox Research Award (to CMG) from Liga Portuguesa Contra o Cancro - LPCC-NRS (Portugal), by Grants FR 1488/3-2 and FR 1488/5-2 from the Deutsche Forschungsgemeinschaft (DFG) (to GF), by the Swedish Medical Research Council, Kempe Foundation, Brain Foundation, and Insamlingsstiftelsen Sweden (to LMR and KY) and a CRUP/DAAD collaborative grant A-15/08 (to CMG and GF).

## REFERENCES

- [1] Marenholz I, Heizmann CW, Fritz G. S100 proteins in mouse and man: from evolution to function and pathology (including an update of the nomenclature). *Biochim Biophys Res Commun* 2004;322:1111–22.
- [2] Marenholz I, Lovering RC, Heizmann CW. An update of the S100 nomenclature. *Biochim Biophys Acta* 2006;1763:1282–3.
- [3] Donato R. Intracellular and extracellular roles of S100 proteins. *Microsc Res Tech* 2003;60:540–51.
- [4] Grevers LC, de Vries TJ, Vogl T, Abdollahi-Roodsaz S, Sloetjes AW, Leenen PJ, et al. S100A8 enhances osteoclastic bone resorption in vitro through activation of Toll-like receptor 4: implications for bone destruction in murine antigen-induced arthritis. *Arthritis Rheum* 2011;63:1365–75.
- [5] Hiratsuka S, Watanabe A, Aburatani H, Maru Y. Tumour-mediated upregulation of chemoattractants and recruitment of myeloid cells predetermines lung metastasis. *Nat Cell Biol* 2006;8:1369–75.
- [6] Hoyaux D, Decaestecker C, Heizmann CW, Vogl T, Schafer BW, Salmon I, et al. S100 proteins in Corpora amylacea from normal human brain. *Brain Res* 2000;867:280–8.
- [7] Salama I, Malone PS, Mihaimed F, Jones JL. A review of the S100 proteins in cancer. *Eur J Surg Oncol* 2008;34:357–64.
- [8] van Lent PL, Grevers L, Blom AB, Sloetjes A, Mort JS, Vogl T, et al. Myeloid-related proteins S100A8/S100A9 regulate joint inflammation and cartilage destruction during antigen-induced arthritis. *Ann Rheum Dis* 2008;67:1750–8.
- [9] Leclerc E, Fritz G, Vetter SW, Heizmann CW. Binding of S100 proteins to RAGE: An update. *Biochim Biophys Acta* 2009;1793:993–1007.
- [10] Vogl T, Tenbrock K, Ludwig S, Leukert N, Ehrhardt C, van Zoelen MA, et al. Mrp8 and Mrp14 are endogenous activators of Toll-like receptor 4, promoting lethal, endotoxin-induced shock. *Nature Med* 2007;13:1042–9.
- [11] Vogl T, Ludwig S, Goebeler M, Strey A, Thorey IS, Reichelt R, et al. MRP8 and MRP14 control microtubule reorganization during transendothelial migration of phagocytes. *Blood* 2004;104:4260–8.
- [12] Yanamandra K, Alexeyev O, Zamotin V, Srivastava V, Shchukarev A, Brorsson AC, et al. Amyloid formation by the pro-inflammatory S100A8/A9 proteins in the ageing prostate. *PLoS One* 2009;4:e5562.
- [13] Fritz G, Botelho HM, Morozova-Roche LA, Gomes CM. Natural and amyloid self-assembly of S100 proteins: structural basis of functional diversity. *FEBS J* 2010;277:4578–90.
- [14] Botelho HM, Leal SS, Cardoso I, Yanamandra K, Morozova-Roche LA, Fritz G, et al. S100A6 amyloid fibril formation is calcium-modulated and enhances superoxide dismutase-1 (SOD1) aggregation. *J Biol Chem* 2012;287:42233–42.
- [15] Rezvanpour A, Shaw GS. Unique S100 target protein interactions. *Gen Physiol Biophys*. 28 Spec No Focus 2009:F39–46.
- [16] Heizmann CW, Fritz G, Schafer BW. S100 proteins: structure, functions and pathology. *Front Biosci* 2002;7:d1356–68.
- [17] Drohat AC, Nenortas E, Beckett D, Weber DJ. Oligomerization state of S100B at nanomolar concentration determined by large-zone analytical gel filtration chromatography. *Protein Sci*. 1997;6:1577–82.
- [18] Ostendorp T, Leclerc E, Galichet A, Koch M, Demling N, Weigle B, et al. Structural and functional insights into RAGE activation by multimeric S100B. *EMBO J* 2007;26:3868–78.
- [19] Vogl T, Leukert N, Barczyk K, Strupat K, Roth J. Biophysical characterization of S100A8 and S100A9 in the absence and presence of bivalent cations. *Biochim Biophys Acta* 2006;1763:1298–306.
- [20] Marlatt NM, Boys BL, Konermann L, Shaw GS. Formation of monomeric S100B and S100A11 proteins at low ionic strength. *Biochemistry* 2009;48:1954–63.
- [21] Deloume JC, Assard N, Mbele GO, Mangin C, Kuwano R, Baudier J. S100A6 and S100A11 are specific targets of the calcium- and zinc-binding S100B protein in vivo. *J Biol Chem* 2000;275:35302–10.
- [22] Leukert N, Vogl T, Strupat K, Reichelt R, Sorg C, Roth J. Calcium-dependent tetramer formation of S100A8 and S100A9 is essential for biological activity. *J Mol Biol* 2006;359:961–72.
- [23] Moroz OV, Burkitt W, Wittkowski H, He W, Ianoul A, Novitskaya V, et al. Both Ca<sup>2+</sup> and Zn<sup>2+</sup> are essential for S100A12 protein oligomerization and function. *BMC Biochem* 2009;10:11.
- [24] Moroz OV, Blagova EV, Wilkinson AJ, Wilson KS, Bronstein IB. The crystal structures of human S100A12 in apo form and in complex with zinc: new insights into S100A12 oligomerisation. *J Mol Biol* 2009;391:536–51.
- [25] Koch M, Diez J, Fritz G. Crystal structure of Ca<sup>2+</sup>-free S100A2 at 1.6 Å resolution. *J Mol Biol* 2008;378:933–42.
- [26] Santamaria-Kisiel L, Rintala-Dempsey AC, Shaw GS. Calcium-dependent and -independent interactions of the S100 protein family. *Biochem J* 2006;396:201–14.
- [27] Fritz G, Mittl PR, Vasak M, Grutter MG, Heizmann CW. The crystal structure of metal-free human EF-hand protein S100A3 at 1.7-Å resolution. *J Biol Chem* 2002;277:33092–8.
- [28] Fritz G, Heizmann CW, Kroneck PM. Probing the structure of the human Ca<sup>2+</sup>- and Zn<sup>2+</sup>-binding protein S100A3: spectroscopic investigations of its transition metal ion complexes, and three-dimensional structural model. *Biochim Biophys Acta* 1998;1448:264–76.
- [29] Koch M, Bhattacharya S, Kehl T, Gimona M, Vasak M, Chazin W, et al. Implications on zinc binding to S100A2. *Biochim Biophys Acta* 2007;1773:457–70.
- [30] Filipek A, Heizmann CW, Kuznicki J. Calyculin is a calcium and zinc binding protein. *FEBS Lett* 1990;264:263–6.
- [31] Dell'Angelica EC, Schleicher CH, Santome JA. Primary structure and binding properties of calgranulin C, a novel S100-like calcium-binding protein from pig granulocytes. *J Biol Chem* 1994;269:28929–36.
- [32] Baudier J, Glasser N, Gerard D. Ions binding to S100 proteins. I. Calcium- and zinc-binding properties of bovine brain S100 alpha alpha, S100a (alpha beta), and S100b (beta beta) protein: Zn<sup>2+</sup> regulates Ca<sup>2+</sup> binding on S100b protein. *J Biol Chem* 1986;261:8192–203.
- [33] Baudier J, Gerard D. Ions binding to S100 proteins: structural changes induced by calcium and zinc on S100a and S100b proteins. *Biochemistry* 1983;22:3360–9.
- [34] Björk P, Björk A, Vogl T, Stenstrom M, Liberg D, Olsson A, et al. Identification of human S100A9 as a novel target for treatment of autoimmune disease via binding to quinoline-3-carboxamides. *PLoS Biol* 2009;7:e97.

- [35] Nishikawa T, Lee IS, Shiraishi N, Ishikawa T, Ohta Y, Nishikimi M. Identification of S100b protein as copper-binding protein and its suppression of copper-induced cell damage. *J Biol Chem* 1997;272:23037–41.
- [36] Mandinova A, Soldi R, Graziani I, Bagala C, Bellum S, Landriscina M, et al. S100A13 mediates the copper-dependent stress-induced release of IL-1alpha from both human U937 and murine NIH 3T3 cells. *J Cell Sci* 2003;116:2687–96.
- [37] Moroz OV, Antson AA, Grist SJ, Maitland NJ, Dodson GG, Wilson KS, et al. Structure of the human S100A12-copper complex: implications for host-parasite defence. *Acta Crystallogr D Biol Crystallogr* 2003;59:859–67.
- [38] Fielding AJ, Fox S, Millhauser GL, Chattopadhyay M, Kroneck PM, Fritz G, et al. Electron spin relaxation of copper(II) complexes in glassy solution between 10 and 120 K. *J Magn Reson* 2006;179:92–104.
- [39] Corbin BD, Seeley EH, Raab A, Feldmann J, Miller MR, Torres VJ, et al. Metal chelation and inhibition of bacterial growth in tissue abscesses. *Science* 2008;319:962–5.
- [40] Kehl-Fie TE, Chitayat S, Hood MI, Damo S, Restrepo N, Garcia C, et al. Nutrient metal sequestration by calprotectin inhibits bacterial superoxide defense, enhancing neutrophil killing of *Staphylococcus aureus*. *Cell Host Microbe* 2011;10:158–64.
- [41] Hofmann MA, Drury S, Fu C, Qu W, Taguchi A, Lu Y, et al. RAGE mediates a novel proinflammatory axis: a central cell surface receptor for S100/calgranulin polypeptides. *Cell* 1999;97:889–901.
- [42] Foell D, Kucharzik T, Kraft M, Vogl T, Sorg C, Domschke W, et al. Neutrophil derived human S100A12 (EN-RAGE) is strongly expressed during chronic active inflammatory bowel disease. *Gut* 2003;52:847–53.
- [43] Xie J, Burz DS, He W, Bronstein IB, Lednev I, Shekhtman A. Hexameric calgranulin C (S100A12) binds to the receptor for advanced glycosylated end products (RAGE) using symmetric hydrophobic target-binding patches. *J Biol Chem* 2007;282:4218–31.
- [44] Malashkevich VN, Dulyaninova NG, Ramagopal UA, Liriano MA, Varney KM, Knight D, et al. Phenothiazines inhibit S100A4 function by inducing protein oligomerization. *Proc Natl Acad Sci USA* 2010;107:8605–10.
- [45] Kiryushko D, Novitskaya V, Soroka V, Klingelhofer J, Lukanidin E, Berezin V, et al. The molecular mechanisms of Ca(2+) signaling in neurons induced by the S100A4 protein. *Mol Cell Biol* 2006;26:3625–38.
- [46] Korndorfer IP, Brueckner F, Skerra A. The crystal structure of the human (S100A8/S100A9)2 heterotetramer, calprotectin, illustrates how conformational changes of interacting alpha-helices can determine specific association of two EF-hand proteins. *J Mol Biol* 2007;370:887–98.
- [47] Lee SW, Tomasetto C, Sager R. Positive selection of candidate tumor-suppressor genes by subtractive hybridization. *Proc Natl Acad Sci USA* 1991;88:2825–9.
- [48] Tartaglia GG, Vendruscolo M. The Zyggregator method for predicting protein aggregation propensities. *Chem Soc Rev* 2008;37:1395–401.
- [49] Maurer-Stroh S, Debulpaep M, Kuemmerer N, Lopez de la Paz M, Martins IC, Reumers J, et al. Exploring the sequence determinants of amyloid structure using position-specific scoring matrices. *Nat Meth* 2010;7:237–42.
- [50] Hoyaux D, Boom A, Van den Bosch L, Belot N, Martin JJ, Heizmann CW, et al. S100A6 overexpression within astrocytes associated with impaired axons from both ALS mouse model and human patients. *J Neuropathol Exp Neurol* 2002;61:736–44.
- [51] Chattopadhyay M, Valentine JS. Aggregation of copper-zinc superoxide dismutase in familial and sporadic ALS. *Antioxidants Redox Signal* 2009;11:1603–14.
- [52] Leal SS, Botelho HM, Gomes CM. Metal ions as modulators of protein conformation and misfolding in neurodegeneration. *Coordination Chem Rev* 2012;256:2253–70.
- [53] Zhang C, Liu Y, Gilthorpe J, van der Maarel JR. MRP14 (S100A9) protein interacts with Alzheimer beta-amyloid peptide and induces its fibrillization. *PLoS One* 2012;7: e32953.
- [54] Botelho HM, Koch M, Fritz G, Gomes CM. Metal ions modulate the folding and stability of the tumor suppressor protein S100A2. *FEBS J* 2009;276:1776–86.
- [55] Paulite M, Fakhraai Z, Li IT, Gunari N, Tanur AE, Walker GC. Imaging secondary structure of individual amyloid fibrils of a beta2-microglobulin fragment using near-field infrared spectroscopy. *J Am Chem Soc* 2011;133:7376–83.
- [56] Li H, Rahimi F, Sinha S, Maiti P, Bitan G, MuraKami K. Amyloids and Protein Aggregation-Analytical Methods. In: Meyers RA, editor. *Encyclopedia of Analytical Chemistry*. Hoboken, NJ: John Wiley; 2009. p. 1–23.
- [57] Malisaukas M, Ostman J, Darinskas A, Zamotin V, Liutkevicius E, Lundgren E, et al. Does the cytotoxic effect of transient amyloid oligomers from common equine lysozyme in vitro imply innate amyloid toxicity? *J Biol Chem* 2005;280:6269–75.
- [58] Jia X, Gharibyan AL, Ohman A, Liu Y, Olofsson A, Morozova-Roche LA. Neuroprotective and nootropic drug noopept rescues alpha-synuclein amyloid cytotoxicity. *J Mol Biol* 2011;414:699–712.
- [59] Saforova K, Dvorak A, Kubinek R, Vujtek M, Rek A. Usage of AFM, SEM and TEM for the research of carbon nanotubes. In: Méndez-Vilas A, Diaz J, editors. *Modern Research and Educational Topics in Microscopy: Extremadura, Spain: Formatex. ; 2007*.
- [60] Anderson VL, Webb WW. Transmission electron microscopy characterization of fluorescently labelled amyloid beta 1-40 and alpha-synuclein aggregates. *BMC Biotechnol* 2011;11:125.
- [61] Cardoso I, Goldsbury CS, Muller SA, Olivieri V, Wirtz S, Damas AM, et al. Transthyretin fibrillogenesis entails the assembly of monomers: a molecular model for in vitro assembled transthyretin amyloid-like fibrils. *J Mol Biol* 2002;317:683–95.
- [62] Costa R, Goncalves A, Saraiva MJ, Cardoso I. Transthyretin binding to A-Beta peptide – impact on A-Beta fibrillogenesis and toxicity. *FEBS Lett* 2008;582:936–42.
- [63] Goldsbury C, Frey P, Olivieri V, Aebi U, Muller SA. Multiple assembly pathways underlie amyloid-beta fibril polymorphisms. *J Mol Biol* 2005;352:282–98.
- [64] Green JD, Goldsbury C, Kistler J, Cooper GJ, Aebi U. Human amylin oligomer growth and fibril elongation define two distinct phases in amyloid formation. *J Biol Chem* 2004;279:12206–12.
- [65] Malisaukas M, Zamotin V, Jass J, Noppe W, Dobson CM, Morozova-Roche LA. Amyloid protofilaments from the calcium-binding protein equine lysozyme: formation of ring and linear structures depends on pH and metal ion concentration. *J Mol Biol* 2003;330:879–90.
- [66] Chiti F, Dobson CM. Protein misfolding, functional amyloid, and human disease. *Annu Rev Biochem* 2006;75:333–66.
- [67] Pawar AP, Dubay KF, Zurdo J, Chiti F, Vendruscolo M, Dobson CM. Prediction of ‘aggregation-prone’ and ‘aggregation-susceptible’ regions in proteins associated with neurodegenerative diseases. *J Mol Biol* 2005;350:379–92.

- [68] Goldsbury C, Kistler J, Aebi U, Arvinte T, Cooper GJ. Watching amyloid fibrils grow by time-lapse atomic force microscopy. *J Mol Biol.* 1999;285:33–9.
- [69] Goldsbury CS, Wirtz S, Muller SA, Sunderji S, Wicki P, Aebi U, et al. Studies on the in vitro assembly of a beta 1-40: implications for the search for a beta fibril formation inhibitors. *J Struct Biol* 2000;130:217–31.
- [70] Untergasser G, Madersbacher S, Berger P. Benign prostatic hyperplasia: age-related tissue-remodeling. *Exp Geront* 2005;40:121–8.
- [71] Yanamandra K, Gruden MA, Casate V, Meskys R, Forsgren L, Morozova-Roche LA. Alpha-synuclein reactive antibodies as diagnostic biomarkers in blood sera of Parkinson's disease patients. *PLoS One* 2011;6:e18513.
- [72] Kaye R, Head E, Sarsoza F, Saing T, Cotman CW, Neucula M, et al. Fibril-specific, conformation-dependent antibodies recognize a generic epitope common to amyloid fibrils and fibrillar oligomers that is absent in prefibrillar oligomers. *Mol Neurodegen* 2007;2:18.